Fast and accurate enzyme activity measurements using a chip-based microfluidic calorimeter

van Schie, Morten; Honarmand Ebrahimi, K.; Hagen, Wilfred R.; Hagedoorn, Peter-Leon

DOI
10.1016/j.ab.2017.12.028

Publication date
2017

Document Version
Final published version

Published in
Analytical Biochemistry

Citation (APA)
van Schie, M., Honarmand Ebrahimi, K., Hagen, W. R., & Hagedoorn, P.-L. (2017). Fast and accurate enzyme activity measurements using a chip-based microfluidic calorimeter. *Analytical Biochemistry*, *544*, 57-63. https://doi.org/10.1016/j.ab.2017.12.028

Analytical Biochemistry 544 (2018) 57–63

Contents lists available at ScienceDirect

Analytical Biochemistry

journal homepage: www.elsevier.com/locate/yabio

Fast and accurate enzyme activity measurements using a chip-based microfluidic calorimeter

Morten M.C.H. van Schie[a], Kourosh Honarmand Ebrahimi[b], Wilfred R. Hagen[a], Peter-Leon Hagedoorn[a,*]

[a] Department of Biotechnology, Delft University of Technology, Van der Maasweg 9, 2629 HZ, Delft, The Netherlands
[b] Department of Chemistry, University of Oxford, South Parks Road, Oxford, OX1 3QR, UK

ARTICLE INFO

Keywords:
Chip-based calorimetry
Enzyme calorimetry
Chemical calibration method
Alkaline phosphatase
Phosphate ionization

ABSTRACT

Recent developments in microfluidic and nanofluidic technologies have resulted in development of new chip-based microfluidic calorimeters with potential use in different fields. One application would be the accurate high-throughput measurement of enzyme activity. Calorimetry is a generic way to measure activity of enzymes, but unlike conventional calorimeters, chip-based calorimeters can be easily automated and implemented in high-throughput screening platforms. However, application of chip-based microfluidic calorimeters to measure enzyme activity has been limited due to problems associated with miniaturization such as incomplete mixing and a decrease in volumetric heat generated. To address these problems we introduced a calibration method and devised a convenient protocol for using a chip-based microfluidic calorimeter. Using the new calibration method, the progress curve of alkaline phosphatase, which has product inhibition for phosphate, measured by the calorimeter was the same as that recorded by UV-visible spectroscopy. Our results may enable use of current chip-based microfluidic calorimeters in a simple manner as a tool for high-throughput screening of enzyme activity with potential applications in drug discovery and enzyme engineering.

Introduction

High-throughput measurement of enzyme activity is dependent on assays that enable time-resolved data collection to record activity of enzymes for a few seconds after addition of substrate. These assays generally require application of UV-visible or fluorescence spectroscopy in order to follow the color or the fluorescence of a substrate or a product [1]. Unfortunately, the natural substrates or products of many enzymes such as phosphatases, proteases, or kinases, do not have a color or are not fluorogenic, and thus, synthetically labeled substrates have to be used. Assays based on labeled synthetic substrates might not represent the true activity of enzymes, which might be misleading in identifying inhibitors as possible drug candidates or understanding the mechanism of the enzymatic reaction [2]. Furthermore, systematic approaches in enzyme engineering, using high-throughput screening for a desired activity, are difficult if the desired enzymatic reaction does not exhibit a color or fluorescence change. This can be solved by chemical or enzymatic coupled reactions, but this requires considerable development and optimization for every targeted enzyme reaction.

Therefore various label-free methods for enzyme activity measurements have been developed, based on different techniques, such as liquid chromatography-mass spectrometry (LC-MS) [3], capillary electrophoresis [4,5], a method based on macrocycle-fluorescent dye complex formation [6], and methods based on heat measurements with isothermal titration calorimetry (ITC) [7]. Recently, a method for time-resolved initial rate measurements using isothermal titration calorimetry (ITC) has been developed as a generic assay for the activity of enzymes. This method is based on a simple calibration reaction and enables accurate initial rate measurements by only recording a few early data points for the heat generated by an enzymatic reaction [8]. Although this method enables fundamental studies of many enzymes with their natural substrates and provides a tool for applying ITC instruments with high-throughput capability in measuring enzyme activity, still enzyme activity measurements using modern ITC instruments are significantly slower compared to those using UV-visible or fluorescence spectroscopy. This is because the ITC instruments, which have a measurement cell of 200–1400 µl, require a thermal equilibration time of 10–20 min to establish isothermal conditions necessary for sensitive measurements.

To address this problem and enable fast equilibration the sample volume required for measurements needs to be decreased. This has been achieved by applying microfluidic technology. New chip-based

* Corresponding author.
E-mail address: P.L.Hagedoorn@tudelft.nl (P.-L. Hagedoorn).

https://doi.org/10.1016/j.ab.2017.12.028
Received 8 June 2017; Received in revised form 14 December 2017; Accepted 18 December 2017
Available online 20 December 2017
0003-2697/

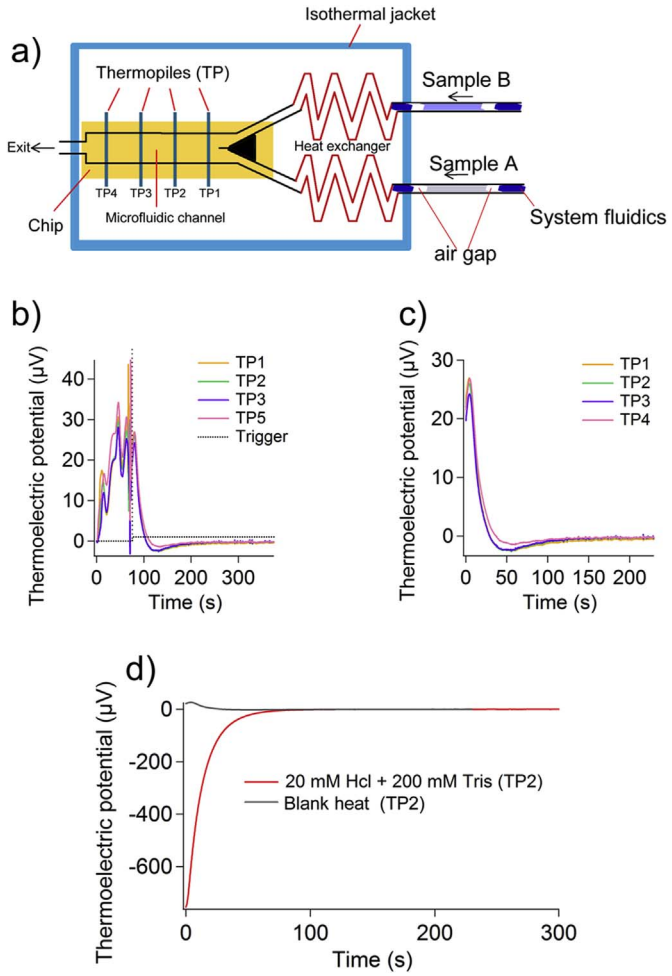

Fig. 1. Measurement of heat using a chip-based microfluidic calorimeter. Data for thermopile 2 are shown and are corrected for the blank heat. Measurements were performed at 37 °C. (a) Schematic representation of a chip-based microfluidic calorimeter. This schematic view is based on the original design by Lerchner et al. [12,13]. The calorimeter consists of a flow cell that is located on a chip with four thermopiles. Each inlet of the microfluidic cell is connected to a heat exchanger. All components are placed in an isothermal jacket. (b) The sample in each inlet to the flow cell is separated from the system fluid (Milli-Q water) using two air gaps, one in front and one in the back. (c) The raw data for measurement of generated thermoelectric potential due to mixing two samples of exactly the same solution of MOPS buffer. The initial data before flow stops are disturbed due to the passage of the air gap and flow over the thermopile. The trigger signal that changes from zero to one, shows the time at which the flow stops and measurements begin. (d) Time zero is set at the trigger signal. (e) The thermoelectric potential generated due to the mixing of 20 mM HCl with 200 mM Tris.

microfluidic calorimeters have been developed [9–11] that have a sample volume of less than 20 µl and a thermal equilibration time of a few seconds. Fig. 1a is a schematic overview of an isothermal chip-based microfluidic calorimeter, which was initially designed by Lerchner et al. [12,13]. In this calorimeter two laminar flows reach the microfluidic cell where heat measurements are made with a set of four thermopiles located in a row directly under the measurement cell. These thermopiles measure the heat based on the heat conduction principle [14]. However, use of this microfluidic calorimeter or other types of chip-based microfluidic calorimeters for accurate measurement of enzyme activity has remained a challenge, due to three inter-related problems: 1) the decrease in volume of the measuring cell and thus the volumetric heat generated compared to conventional ITC instruments, 2) the lack of complete mixing in a sufficiently short time [15], and 3) the lack of calibration methods to translate heat measurements into enzyme activity.

To address the above problems, we have applied a chip-based microfluidic calorimeter (Fig. 1a) for enzyme activity measurements. We developed a new calibration method which enabled the use of simple calculations to accurately determine the activity of enzymes. Practical application of this calibration method was demonstrated for alkaline phosphatase, which catalyses the dephosphorylation of different substrates [16] and is a target for drug discovery [17].

Methods

Chemicals

3-morpholinopropane-1-sulfonic acid (MOPS), *para*-nitrophenyl phosphate (PNPP) and HCl were obtained from Sigma-Aldrich. KCl, and Tris were obtained from Merck. NaCl, NaOH, KH_2PO_4 and $MgCl_2$ were obtained from J.T. Baker. Alkaline phosphatase from bovine intestinal mucosa was purchased from Sigma-Aldrich.

Microfluidic calorimeter experiments

A chip-based microfluidic calorimeter (ChipCAL) was used (TTP Labtech). For each experiment the solutions were filtered on 0.45 µm Whatman filters (GE Healthcare) and were degassed prior to injection into the microfluidic cell in order to prevent formation of air bubbles. After each experiment the microfluidic cell was washed with Milli-Q water. At the end of a set of experiments, before turning the instrument off, the microfluidic cell was cleaned by further washing with Milli-Q water. Of the four thermopiles registering the heat changes only the data of thermopile 2 were used. Thermopile 1 and 4 were not considered in view of occasional disturbance of the measurement due to air bubbles at the end or beginning of the flow cell. Thermopile 3 gave similar results as thermopile 2.

Isothermal titration calorimetry

A VP-ITC from Microcal (Malvern) with a cell of 1.4 ml was used to perform isothermal titration calorimetry (ITC) experiments. The instrument settings were: high feedback mode, stirring speed 502 rpm, reference power 63 µJ/s and a filtering time of 2 s. The instrument was calibrated electrically using the procedure provided by the maker. This calibration procedure involved the administration of a defined power to a resistive heater located next to the measurement cell. Samples were degassed and heated up to reaction temperature before the experiment. At the beginning of each experiment 2 µl of the sample was injected into the cell. The data point resulting from this injection was discarded in view of inaccuracy in the volume and sample concentration in the first injection. Subsequently 3 µl of the sample was injected twice to obtain two measurements for the reaction enthalpy. For the Tris-HCl calibration experiments the sample in the syringe contained a 1 mM HCl solution in Milli Q, while the cell contained a 200 mM Tris solution at pH 10.6. For the phosphate calibration experiments the sample in the syringe contained a 10 mM KPi solution in a 200 mM MOPS, 20 mM NaCl buffer at pH 5, while the cell contained a 200 mM MOPS, 20 mM NaCl solution at pH 8. The experiment was designed such that the heat developed after the injection had dissipated and the signal returned to the baseline before the next injection. Samples were degassed and heated to the experimental temperature prior to all experiments. The dilution enthalpy of the sample was determined and subtracted from the reaction enthalpy as a blank. The integral of the obtained curve was taken as the reaction enthalpy.

Calibration sample preparation

To test the suitability of several calibration methods, the following solutions were injected into the ChipCAL: 1) 200 mM Tris solution, pH 10.6 versus 5–20 mM HCl in Milli Q water; 2) 200 mM MOPS 20 mM NaCl pH 8.0 versus 5–20 mM KH_2PO_4 in 200 mM MOPS 20 mM NaCl

pH 5.0. To determine the enthalpy of dilution, the individual samples were injected versus Milli Q water. All experiments were done at least in triplicate. When repeating experiments, the solutions were prepared freshly before each experiment.

Enzymatic essays

Alkaline Phosphatase (AP) from bovine intestinal mucosa was used to convert *para*-nitrophenyl phosphate (PNPP) into *para*-nitrophenol (PNP) and phosphate. The Michaelis-Menten kinetics for the enzyme under these condition were determined using the following UV-vis assay. The initial rate of conversion of 5–400 μM of PNPP by 0.07 nM of alkaline phosphatase was determined in a 200 mM Tris buffer at pH 8.5. The formation of PNP was measured at 405 nm ($\varepsilon = 18 \cdot 10^3\,M^{-1}\,cm^{-1}$). In the experiments to compare the measurements from the ChipCAL and from UV-vis spectroscopy, 10 nM of alkaline phosphatase was used to convert 5 mM of PNPP. For this experiment the buffer was a 200 mM Tris buffer at pH 8.5. The PNP formation was followed by measuring the absorbance at 480 nm ($\varepsilon = 0.18 \cdot 10^3\,M^{-1}\,cm^{-1}$). For inhibition studies, 2 mM phosphate was added to the reaction mixture. Due to the introduction of two equal sample volumes in the ChipCAL measuring cell, the samples were diluted twofold. To compensate for this, a solution of 20 nM alkaline phosphatase was injected as one sample and a 10 mM PNPP, with or without 4 mM phosphate as the other. For the ITC experiments, in order to determine the enthalpy for this reaction, the sample in the syringe contained 10 mM PNPP in a 200 mM Tris buffer at pH 8.5. The cell contained a 10 nM AP solution in a 200 mM Tris buffer at pH 8.5. For the blank measurement the enzyme was omitted.

Diffusion coefficient calculation

The standard diffusion coefficients of different salts and the correction for temperature were calculated using data from the handbook of chemistry and physics and equation (1).

$$Dc = \frac{(z_+ + |z_-|) * D_+ * D_-}{z_+ * D_+ + z_- * D_-} \quad (1)$$

Here, D_+ and D_- are the partial diffusion coefficients of the cation and the anion and z_+ and z_- their respective charge numbers. Diffusion coefficients at 37 °C were predicted by correcting the standard coefficients by an increase of 2.5% per degree.

Results and discussion

Heat flow measurements using a chip-based microfluidic calorimeter

In the chip-based microfluidic calorimeter of Fig. 1a, which was used in the present work, two samples of 18 μl are drawn by two syringe pumps. The system fluid (Milli-Q water) guides the sample in each syringe with a flow rate of 75 μl min^{-1} to the microfluidic channel. Under these conditions the Reynolds number is in the order of 10^2, consistent with laminar flow. To prevent mixing of the sample with the system fluid, air gaps of 2 μl are introduced before and after the sample plug. The two liquids pass through a heat exchanger for thermal equilibration before reaching the microfluidic channel. As soon as the front air gap reaches the end of the microfluidic cell (channel), the flow stops and measurement begins (Fig. 1b). The microfluidic channel where heat measurements are taking place, is located in an isothermal environment and is placed onto a chip containing four thermopiles and has a volume of 18 μl. Because of the laminar flow of the samples and no other means of active mixing, the samples in the measuring cell are mixed due to diffusion [18]. A change in temperature within the channel induces a thermoelectric potential (μV) which is recorded by the instrument. Each thermopile measures this change in temperature individually. The time required to fill the microfluidic channel is 7.2 s. The dead time, i.e. the time that the two samples have been in contact before the flow is stopped, for thermopiles 1, 2, 3 and 4 is 0.9, 2.7, 4.5 and 6.3 s respectively. In total, approximately 80 s after injecting the samples into the microfluidic system, the measurement in the cell starts.

We recorded the change in heat generated in the cell caused by the flow of two identical liquids, i.e. MOPS buffer (Fig. 1c). Before the flow stops, which is marked by a trigger signal, the measurement is very noisy due to the passage of the front air gap and the flow. Thus, only the data collected after the flow has stopped are useful (Fig. 1d). The change in temperature inside the microfluidic cell was recorded as a time dependent thermoelectric potential (μV). The signal returned to baseline, zero thermoelectric potential, as the temperatures inside and outside the microfluidic cell became equal. Subsequently, to test the response of the microfluidic calorimeter, we recorded the heat generated due to the mixing of HCl with Tris buffer. To obtain the heat generated only due to the reaction of HCl with Tris, the blank was subtracted. The final results for one of the thermopiles (Thermopile 2) are shown in Fig. 1e. A significant drop in thermoelectric potential as compared to the blank was observed. Because the recorded thermoelectric potential is negative, the results show that the reaction was exothermic. By ITC it was established that the enthalpy for this reaction was $-49.7\,kJ\,mol^{-1}$. In literature an enthalpy of $-47.45\,kJ\,mol^{-1}$ is reported [19].

Response time of microfluidic calorimeter is diffusion dependent

We then recorded the response of each thermopile to the heat generated by four different reactions: Tris-HCl reaction, dilution of 1 M NaCl, dilution of 1 M KCl, and dilution of 1 M KH_2PO_4, and the results were corrected for the blank (Fig. 2a and Supplementary Fig. S1). While the reaction of Tris-HCl is exothermic, the dilutions of KCl, NaCl, and KH_2PO_4 are endothermic. For each reaction the recorded thermoelectric potential as a function of time could be fitted to a single exponential decay. Thus, the data were fitted using equation (2) (Fig. 2a):

$$\boldsymbol{f(t) = A \cdot e^{-k \cdot t} + c} \quad (2)$$

In this equation k is a first order rate constant (s^{-1}). A is the initial offset of the data and can have a negative or a positive value depending on whether the reaction was exothermic or endothermic respectively. It was found that the rate constant (k) was different for each reaction. As stated before, in the microfluidic channel where the two laminar flows enter, active mixing does not occur. This means that the small molecules (i.e. not biomacromolecules) present in each flow mainly disperse by diffusion, which is dependent on the diffusion coefficient of each molecule in a specific solution, as is described by equation (3).

$$\boldsymbol{x^2 = 2 \cdot D_c \cdot t} \quad (3)$$

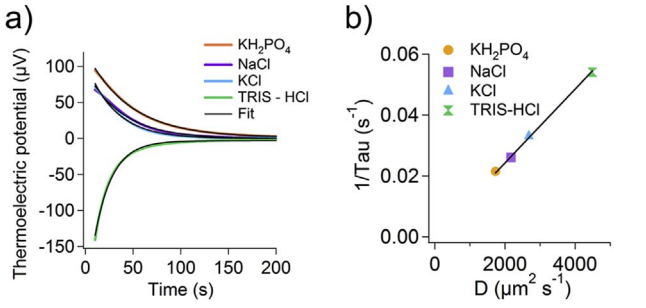

Fig. 2. The response of thermopiles is affected by diffusion. (a) The thermoelectric potential was measured for four different reactions: reaction of 200 mM Tris and 5 mM HCl (green), or dilution of 5 mM KCl (blue), 5 mM NaCl (purple), or 5 mM KH_2PO_4 (orange) in water. All measurements were performed at 37 °C. The black line shows the fit to an exponential decay (equation (2)). All graphs are for thermopile 2. (b) A plot of rate constant (k) as a function of diffusion coefficient. For the Tris-HCl reaction the diffusion coefficient is for HCl. (For interpretation of the references to color in this figure legend, the reader is referred to the Web version of this article.)

Here, D_c is the diffusion coefficient of the molecule and x is the root mean square displacement. It was concluded that the difference in the response of the microfluidic calorimeter to the heat generated by each reaction was due to the absence of active mixing. In other words, the rate constant (k) in equation (2) for each thermopile is affected by the diffusion rate of the compounds. For each compound the rate constants (k) were plotted as a function of the calculated diffusion coefficient (Fig. 2b) (supporting information Table S1) [20]. The reaction of Tris with HCl is determined by proton exchange, which is instantaneous in the timeframe of the measurements. The diffusion of protons in aqueous solution is unusually fast, which has been explained by the Grotthuss mechanism [21]. This theory states that, rather than through Brownian motion, protons can move through an aqueous solution by sequential hydrogen bond formation and covalent bond cleavage. Therefore, the diffusion rate of Tris is negligible compared to that of HCl. It can be concluded that the greater the diffusion coefficient, the greater k will be. Hence, k can be used as an indication to approximate how much time is needed for near complete mixing due to the diffusion of small molecules.

Conventional calibration methods are not suitable for calibrating the microfluidic calorimeter

To convert the output signal of the microfluidic calorimeter to the power (W) generated, i.e. the rate of heat (J/s) produced or consumed by a reaction, we need to know the effective sensitivity S_{TP} (V/W) of each thermopile. To determine the effective sensitivity of each thermopile we used the Tris-HCl reaction, which has been widely applied for calibration of calorimeters [22,23]. Different amounts of HCl were mixed with 200 mM Tris, and the output of each thermopile, which is in μV as a function of time, was obtained after correction for the blank heat (Fig. 3a). For the Tris-HCl reaction, the response of each thermopile was different. To obtain the sensitivity of each thermopile, the integrated thermal potential for each thermopile (μV·s) was plotted as a function of the amount of HCl (μmole) added (Fig. 3b–e). The measured potential over time compared to the amount of reactant added can be used to obtain the sensitivity of each thermopile using equation (4):

$$S_{TP}\left(\frac{V}{W}\right) = \frac{Slope\left(\frac{\mu V \cdot s}{mole}\right)}{\Delta H\left(\frac{\mu J}{mole}\right)} \quad (4)$$

in which ΔH (μJ/mole) is the enthalpy of the reaction, which was obtained using isothermal titration calorimetry (ITC). Reaction enthalpies obtained from ITC were preferred over literature values since the enthalpy can change with experimental conditions. We applied the same experimental conditions for the ITC and the microfluidic calorimeter. The final value for the sensitivity of each thermopile is given in Table 1. The sensitivity among the four thermopiles varies significantly, which can be related to the design of the calorimeter. Measurements start when the flow reaches the end of the flow cell and thus the segments of the samples that reach the last thermopile have been in contact for a longer time than the segments of the flow that is measured by the thermopile 1 (Fig. 1a). Therefore, for the reaction taking place near the fourth thermopile (TP4, Fig. 1a) some heat was already dissipated through the other thermopiles during the filling of the channel. On the contrary, the flow coming together near the first thermopile do so shortly after entering the flow-cell and therefore, the first thermopile (TP1) experiences more of the reaction. Because of the extremely fast diffusion of protons and the difference in the dead-time of each thermopile, different sensitivities are obtained when the Tris-HCl reaction is used. Furthermore, the experimental errors in the sensitivity values that were obtained using Tris-HCl and shown as standard deviation (SD) (Table 1) were up to 50%, which suggest poor reproducibility. Therefore we concluded that the Tris-HCl reaction is not an appropriate model reaction for the development of a calibration method for the microfluidic calorimeter.

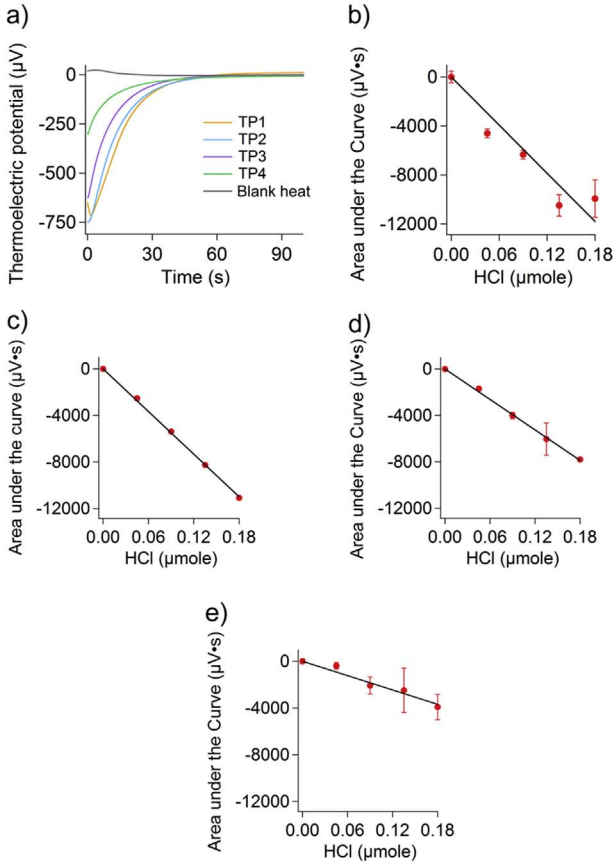

Fig. 3. Tris-HCl reaction is not practical for calibration of chip-based microfluidic calorimeter. (a) The thermoelectric potential recorded by each thermopile due to the mixing of 200 mM Tris and 20 mM HCl in the microfluidic cell. (b) The plot of area under the curve for the reaction of 200 mM Tris with different amounts of HCl as a function of μmole HCl added for thermopile 1 (TP1), (c) for thermopile 2 (TP2), (d) for thermopile 3 (TP3), and (e) for thermopile 4 (TP4). Measurements were performed at 37 °C.

Table 1
The calculated sensitivity of each thermopile for two different reactions.

Thermopile	Sensitivity (V/W)	
	Tris-HCl	P_i deprotonation
TP1	1.38 ± 0.24	1.14 ± 0.09
TP2	1.22 ± 0.01	1.11 ± 0.06
TP3	0.90 ± 0.04	1.05 ± 0.06
TP4	0.56 ± 0.30	0.93 ± 0.06

The sensitivity of each thermopile was obtained from the slope of the data for area under the curve as a function of amount (μmole) of HCl or Pi added, and using equation (4). Each value is the average of measurements at three different days each performed in triplicate ± standard deviation. All solutions were prepared freshly for each measurement to check reproducibility.

An accurate calibration method using deprotonation of phosphate

To find a proper calibration reaction, which, unlike the Tris-HCl reaction, provides a more homogenous heat distribution along the microfluidic cell, we tested reactions of compounds having smaller diffusion coefficients than that of protons in the Tris-HCl reaction. Among different reactions tested we found that the deprotonation of phosphate provides an ample amount of heat over an appreciable amount of time (on the order of minutes). Thus, this reaction was chosen to determine the sensitivity of each thermopile. To measure the deprotonation of phosphate, it was dissolved in 200 mM MOPS at pH 5.0 and was mixed in the channel with a 200 mM MOPS solution at pH 8.0, which results in

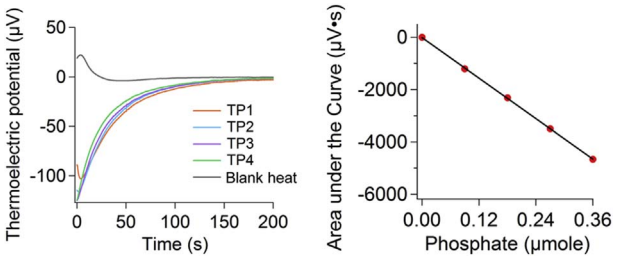

Fig. 4. An accurate calibration method for converting the thermoelectrical potential recorded by each thermopile to the rate of heat generated by a reaction. Left: Deprotonation of phosphate was measured after mixing of 40 mM phosphate in 200 mM MOPS, 20 mM NaCl pH 5.0 with 200 mM MOPS 20 mM NaCl pH 8. Right: The plot of the area under the curve for thermopile 2 for the deprotonation of phosphate. Measurements were performed at 37 °C.

a final pH of 7.1. This is close to the pK_a of $H_2PO_4^-/HPO_4^{2-} + H^+$ (7.2), so one would expect considerable deprotonation. Using ITC, an enthalpy of -10.2 ($\pm$ 0.35) kJ mol^{-1} was found for this partial ionization of phosphate. By calculating the partial ionization of phosphate and the ionization enthalphies for phosphate and MOPS, the reaction enthalpy was calculated to be $-8.2\,kJ\,mol^{-1}$ (see supplementary information). This value is based on literature values for the phosphate pK_a ($pKa = 7.2$) and the ionization enthalpy for phosphate ($\Delta H_{i,Pi} = 2.15\ kJ/mol$ at 37 °C) and MOPS ($\Delta H_{i,MOPS} = 21.1\ kJ/mol$ at 25 °C) [19]. The response of the microfluidic calorimeter to the deprotonation reaction of phosphate is shown in Fig. 4. Similar changes in temperature were detected by all thermopiles, suggesting near complete homogenous heat distribution over the full length of the cell. A plot of the area under the curves as a function of the moles of Pi added is shown in Fig. 4 and the slope was used to obtain the sensitivity of each thermopile using equation (4) (Table 1). The sensitivities of the four thermopiles vary significantly less than was the case for the Tris-HCl method (Table 1). On the other hand it can be observed that the deprotonation of phosphate as a calibration method gives reproducible results. In conclusion, use of phosphate as a calibration method for obtaining the sensitivity factor of each thermopile is preferred over the conventional method of using Tris-HCl.

Theoretical consideration for enzyme kinetic measurements

Based on mass balance calculations over the flow-cell we conclude that one should pay extra attention to the concentration of the substrate over the width of the flow cell in order to understand the conditions required for homogenous heat distribution. From the previous experiments it was concluded that mixing in the microfluidic channel is almost purely dependent on the diffusion rate, which in turn is dependent on the diffusion coefficient and the concentration of the compounds. However, when performing enzyme kinetic measurements, simultaneously with diffusion, the substrate will also be converted by the enzyme present, which will influence the substrate gradient within the flow cell. At low substrate concentrations, this conversion will result in a lower observed enzyme activity when the substrate has diffused throughout the flow cell. For accurate determination of the enzyme performance the conversion rate should be close to V_{max}. As a consequence, the K_M of the reaction can only be determined if the conversion at substrate concentrations below the K_M can be kept to a minimum during the substrate diffusion time. This will only be possible if the $\Delta H_{reaction}$ and K_M are large and the rate is relatively low. One way to circumvent this challenge altogether, would be the introduction of rapid active mixing of the two samples before entering the flow cell. However, this would most likely also introduce another factor, generation of heat due to friction, which would further complicate the system and decrease its accuracy. Further research is needed to investigate whether fast mixing without introducing friction would be possible.

The translational diffusion coefficient of a compound is inversely proportional to the diameter of the molecule. Thus, for a protein of large size the diffusion coefficient is very small and its diffusion can be considered negligible in the timeframe of the measurement. Combined with the fact that enzyme concentrations used in typical experiments are in the order of micro-to nanomolar, the heat of dilution of the enzyme should be negligible in this instrument. This prediction was confirmed by measuring the heat of dilution of a concentrated BSA solution (Supplementary Fig. S2). The diffusion coefficient of BSA is $6.0 \cdot 10^{-7}\ cm^2\,s^{-1}$ [24]. According to equation (3), the average diffusion of a BSA molecule over 0.5 mm (half the width of the measurement cell) would take hours. Under the conditions that both the concentration and the diffusion coefficient of enzyme [25] are orders of magnitude lower than that of the substrate, it can be assumed that for several minutes after the start of an enzymatic reaction, the enzyme molecules do not diffuse significantly. As a result, half of the volume of the cell is occupied with enzyme (Fig. 5) and is effective in heat production due to the enzymatic reaction.

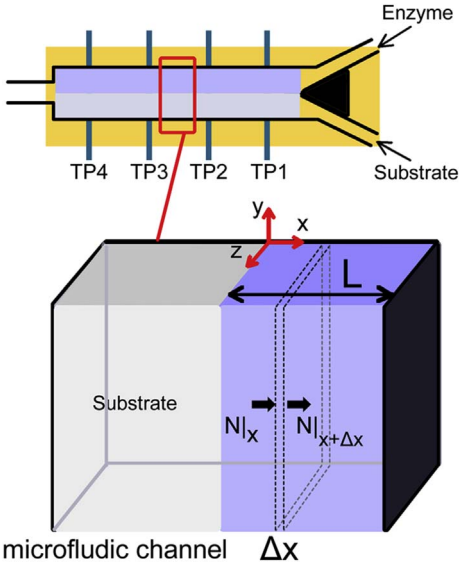

Fig. 5. Diffusion profile of substrate in the enzyme solution. The solution that contains the enzymes occupies half of the microfluidic cell. Because the enzyme does not significantly diffuse, half of the total volume of the microfluidic cell should be considered in heat production and enzyme activity measurements. By writing the mass balance for substrate, the concentration profile of substrate in the enzyme solution can be obtained.

On the other hand, assuming a homogenous substrate solution before entering the flow cell, the concentration profile of substrate in the enzymatic film can be obtained by writing the mass balance equation:

$$(\boldsymbol{N}|_{\boldsymbol{x}} \cdot \boldsymbol{A}) - (\boldsymbol{N}|_{\boldsymbol{x}+\Delta \boldsymbol{x}} \cdot \boldsymbol{A}) - (\boldsymbol{R} \cdot \boldsymbol{A} \cdot \Delta \boldsymbol{x}) = 0 \quad (5)$$

in which x is the vector as shown in Fig. 5, $N|_x$ is the flux of substrate in, $N|_{x+\Delta x}$ is the flux of substrate out, A is the area over which substrate diffuses and R is the rate of consumption of substrate by the enzymatic reaction, which can be expressed by the Michaelis-Menten equation:

$$\boldsymbol{R} = \frac{\boldsymbol{V_{max}} \cdot \boldsymbol{C_s}}{\boldsymbol{K_M} + \boldsymbol{C_s}} \quad (6)$$

in which C_s is the concentration of substrate. By substituting equation (6) into equation (5), dividing by Δx, and letting Δx→0, we can write:

$$\lim_{\Delta x \to 0} \left(\frac{\boldsymbol{N}|_{x+\Delta x} - \boldsymbol{N}|_{x}}{\Delta \boldsymbol{x}} \right) = -\frac{\boldsymbol{V_{max}} \cdot \boldsymbol{C_s}}{\boldsymbol{K_M} + \boldsymbol{C_s}} \quad (7)$$

$$\frac{\boldsymbol{dN}}{\boldsymbol{dx}} = -\frac{\boldsymbol{V_{max}} \cdot \boldsymbol{C_s}}{\boldsymbol{K_M} + \boldsymbol{C_s}} \quad (8)$$

For the diffusive flux we can write Fick's law:

$$N = -D\frac{dC_s}{dx} \tag{9}$$

And thus we have:

$$\frac{d\left(-D\frac{dC_s}{dx}\right)}{dx} = -\frac{V_{max}\cdot C_s}{K_M + C_s} \Rightarrow \frac{d^2C_s}{dx^2} = \frac{\frac{V_{max}}{D}\cdot C_s}{K_M + C_s} \tag{10}$$

To simplify the above equation, we work under the condition that the amount of substrate added is much greater than the K_M of enzyme and therefore the rate is V_{max}, thus we have:

$$\frac{d^2C_s}{dx^2} = \frac{V_{max}}{D} \tag{11}$$

To solve equation (11), two boundary conditions are known:

1. At x = 0, we have $C_S = C_{S0}$
2. At x = L (beyond the cell), we have $\frac{dC_s}{dx} = 0$

Using these boundary conditions we obtain the equation for the concentration profile of substrate in the part of the cell containing the enzyme:

$$C_S = \frac{V_{max}}{2\cdot D}x^2 + \frac{-V_{max}\cdot L}{D}x + C_{S0} \tag{12}$$

This equation suggests that at x = L the concentration of substrate will be:

$$C_S = \frac{-V_{max}\cdot L^2}{2D} + C_{S0} \tag{13}$$

in which L is 0.5 mm and D is in the range of 0.5–2.0 · 10^{-5} $cm^2\,s^{-1}$. Therefore, for enzyme kinetic measurements C_{S0} should be chosen such that C_S at x = L remains greater than the K_M of the enzyme. Under this condition we may assume homogenous heat production through the flow cell half containing the enzyme.

Accurate measurement of enzyme progress curves using chip-based microfluidic calorimeter

The microfluidic calorimeter was applied to measure activity of an enzyme, the hydrolysis of PNPP by 10 nM of alkaline phosphatase to PNP and phosphate at a substrate concentration of 5 mM. The product phosphate inhibits the activity of enzyme. The enthalpy for this reaction was determined by ITC to be −43.7 kJ mol^{-1}. The literature value for hydrolysis of PNPP by alkaline phosphatase at pH 8.5 and 25 °C is −43.2 kJ mol^{-1} [26]. By UV-visible spectroscopy, for an alkaline phosphatase concentration of 0.067 nM, k_{cat} was determined to be (3.58 ± 0.15)·10^3 s^{-1} and the K_M to be 35 ± 4 μM. Following equation (13), the substrate concentration remains well above the K_M. The output of the microfluidic calorimeter for conversion of PNPP by alkaline phosphatase, which is an exothermic reaction, was recorded and the results were corrected for the blank and dilution of substrate in buffer (Fig. 6a). The initial drop in the thermoelectric potential (Fig. 6a), which took circa 50 s, is possibly due to the initial diffusion of substrate in the enzyme layer. This length of time is consistent with the earlier observations for the diffusion of different small molecules (Fig. 2b). Subsequently, using the sensitivity factor that we obtained for phosphate, the output signal was converted to μJ/s and was plotted as a function of time (Fig. 6b). To obtain the rate of the enzyme at each data point we used the following equation:

$$Rate_{Enz} = \frac{power\left(\frac{\mu J}{s}\right)}{\Delta H\left(\frac{\mu J}{\mu mol}\right)\cdot V} \tag{14}$$

in which V is the volume of the microfluidic cell that is occupied by enzyme, which is approximately half of the total volume of the cell (9 μl). The final results are shown in Fig. 6c. To test the accuracy of the

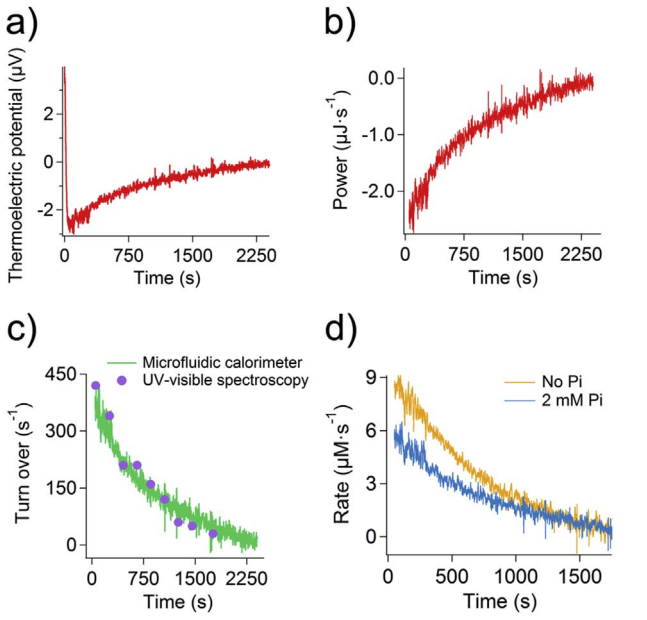

Fig. 6. Accurate enzyme activity measurement using a chip-based microfluidic calorimeter. All graphs are for thermopile 2. (a) Thermoelectric potential recorded after injection of 9 μl of 4 mM PNPP and 9 μl of 20 nM alkaline phosphatase. The data are corrected for heat of dilution and the heat of the blank. Measurements were performed at 37 °C. (b) Using the thermopile sensitivity factor obtained from the deprotonation of phosphate the thermoelectric potential recorded for conversion of PNPP by alkaline phosphatase was converted to power (μJ/s). These data were used to obtain the rate of reaction at each time point (c) with equation (14). (d) Effect of phosphate, which is an inhibitor of alkaline phosphatase, on the rate of enzymatic reaction after injection of 9 μl of 4 mM PNPP and 9 μl of 20 nM alkaline phosphatase. Both substrate and enzyme solutions contained 2 mM phosphate.

results obtained, the conversion of PNPP by alkaline phosphatase was measured under exactly the same conditions using UV-visible spectroscopy. Due to continuous formation of phosphate, which inhibits the activity of alkaline phosphate with a K_i = 1.55 μM [27,28], the progress curves measured by UV-visible and microfluidic calorimeter showed a continuous decrease in the rate. Using the slope of the progress curve of conversion of PNPP by alkaline phosphatase for time intervals of 200 s (Fig. 6d), and knowing the molar extinction coefficient of PNP, the rates of enzymatic reaction were compared with those obtained using calorimetry (Fig. 6c). It can be seen that the results obtained from the chip-based microfluidic calorimeter are within experimental error the same as those obtained using UV-visible spectroscopy. We then checked if the microfluidic calorimeter could be used for identifying inhibition of an enzyme. To this goal conversion of PNPP by alkaline phosphatase was measured in the presence and the absence of phosphate. The recorded thermoelectric potential curves were converted to the rate of enzyme using the sensitivity factor obtained by the phosphate calibration method and making use of equation (14). The final results are shown in Fig. 6d. It can be seen that the chip-based microfluidic calorimeter can also be used to measure enzyme inhibitors.

Conclusions

Our data collectively show that using an accurate and simple calibration method and applying the assumption that the diffusion of an enzyme is negligible relative to its small molecule substrates, a major problem of the microfluidic calorimeters for enzyme activity measurements, namely insufficient mixing due to miniaturization, can be overcome for enzymes with a single substrate. As an example, we showed that the activity of alkaline phosphatase with PNPP as measured by microfluidic calorimeter matched well to that measured by UV-visible spectrometry. Moreover, the sensitivity of our setup allowed

measuring the inhibitory effect of phosphate on the activity of alkaline phosphatase. Therefore, we predict that our method to calibrate the microfluidic calorimeter and our suggested experimental design will allow convenient use of microfluidic calorimeters for high-throughput and accurate measurement of enzyme activity using natural substrates for screening purposes, e.g. for screening of enzyme inhibitors as possible drug candidates or in identifying new mutants of an enzyme with improved activity. The identified inhibitors or enzyme mutants can further be characterized using more sensitive methods such as isothermal titration calorimetry.

However some limitations remain to be addressed. Although we have solved the problem associated with mixing for enzymes with a single small molecule substrate, our approach cannot be used for enzymes whose substrate is a larger peptide or a protein, since these molecules will diffuse slowly. Moreover, the volumetric heat generated in microfluidic calorimeters is considerably lower compared with isothermal titration calorimeters because the volume of the microfluidic cell ($< 20\,\mu l$) is 10-fold less. Although this limitation might be addressed to some extent by increasing the enzyme and substrate concentration, the application of microfluidic calorimeters to certain enzymes (in particular catalyzing reactions with an enthalpy change significantly less than the enthalpy of dilution of substrate, like for most isomerases) is not yet possible and further improvement of the sensitivity is required.

Competing financial interests

MMCHvS, KHE, WRH and PLH declare competing financial interests in the form of a pending patent application with the title “A new calibration method for Chip-based microfluidic calorimeters”.

Acknowledgements

We thank Dr. Denise Jacobs (DSM), Simon Leygeber and Prof. dr. Thomas Hankemeier (LACDR, Leiden University) for their contribution with discussion on this project. We thank Marc Stampraad for technical assistance. This work was financially supported by the BE-BASIC foundation (FS01-013) (www.be-basic.org).

Appendix A. Supplementary data

Supplementary data related to this article can be found at http://dx.doi.org/10.1016/j.ab.2017.12.028.

References

[1] J.P. Goddard, J.L. Reymond, Enzyme assays for high-throughput screening, Curr. Opin. Biotechnol. 15 (2004) 314–322.
[2] M. Rangl, L. Rima, J. Klement, A. Miyagi, S. Keller, S. Scheuring, Real-time visualization of phospholipid degradation by outer membrane phospholipase A using high-speed atomic force microscopy, J. Mol. Biol. 429 (2017) 977–986.
[3] T. de Rond, M. Danielewicz, T. Northen, High-throughput screening of enzyme activity with mass spectrometry imaging, Curr. Opin. Biotechnol. 31 (2015) 1–9.
[4] X. Wang, K. Li, E. Adams, A.V. Schepdael, Recent advances in CE-mediated microanalysis for enzyme study, Electrophoresis 35 (2014) 119–127.
[5] G.K.E. Scriba, F. Belal, Advances in capillary electrophoresis-based enzyme assays, Chromatographia 78 (2015) 947–970.
[6] A. Hennig, H. Bakirci, W.M. Nau, Label-free continuous enzyme assays with macrocycle-fluorescent dye complexes, Nature Methods 4 (2007) 629–632.
[7] F. Bianchi, A.P. Praplan, N. Sarnela, J. Dommen, A. Kurten, I.K. Ortega, S. Schobesberger, H. Junninen, M. Simon, J. Trostl, T. Jokinen, M. Sipila, A. Adamov, A. Amorim, J. Almeida, M. Breitenlechner, J. Duplissy, S. Ehrhart, R.C. Flagan, A. Franchin, J. Hakala, A. Hansel, M. Heinritzi, J. Kangasluoma, H. Keskinen, J. Kim, J. Kirkby, A. Laaksonen, M.J. Lawler, K. Lehtipalo, M. Leiminger, V. Makhmutov, S. Mathot, A. Onnela, T. Petaja, F. Riccobono, M.P. Rissanen, L. Rondo, A. Tome, A. Virtanen, Y. Viisanen, C. Williamson, D. Wimmer, P.M. Winkler, P.L. Ye, J. Curtius, M. Kulmala, D.R. Worsnop, N.M. Donahue, U. Baltensperger, Insight into acid-base nucleation experiments by comparison of the chemical composition of positive, negative, and neutral clusters, Environ. Sci. Technol. 48 (2014) 13675–13684.
[8] K.H. Ebrahimi, P.L. Hagedoorn, D. Jacobs, W.R. Hagen, Accurate label-free reaction kinetics determination using initial rate heat measurements, Sci. Rep. 5 (2015) 16380.
[9] W. Lee, J. Lee, J. Koh, Development and applications of chip calorimeters as novel biosensors, Nanobiosensors Dis. Diagnosis (2012) 17–29.
[10] S. Wang, Micro-differential scanning calorimeter for liquid biological samples, Rev. Sci. Instrum. 87 (2016) 105005.
[11] M. Ahrenberg, E. Shoifet, K.R. Whitaker, H. Huth, M.D. Ediger, C. Schick, Differential alternating current chip calorimeter for in situ investigation of vapor-deposited thin films, Rev. Sci. Instrum. 83 (2012) 033902.
[12] J. Lerchner, T. Maskow, G. Wolf, Chip calorimetry and its use for biochemical and cell biological investigations, Chem. Eng. Process: Process Intensification 47 (2008) 991–999.
[13] V. Baier, R. Födisch, A. Ihring, E. Kessler, J. Lerchner, G. Wolf, J.M. Köhler, M. Nietzsch, M. Krügel, Highly sensitive thermopile heat power sensor for microfluid calorimetry of biochemical processes, Sensor Actuator Phys. 123–124 (2005) 354–359.
[14] S. Kasap, Thermoelectric effects in metals: thermocouples, http://kasap3.usask.ca/samples/Thermoelectric-Seebeck.pdf, (2001) , Accessed date: 8 June 2017.
[15] G.M. Whitesides, The origins and the future of microfluidics, Nature 442 (2006) 368–373.
[16] A. Garen, A fine-structure genetic and chemical study of the enzyme alkaline phosphatase of *E. coli*, Biochim. Biophys. Acta 38 (1959) 470–483.
[17] J.B. Park, D.Y. Kang, H.M. Yang, H.J. Cho, K.W. Park, H.Y. Lee, H.J. Kang, B.K. Koo, H.S. Kim, Serum alkaline phosphatase is a predictor of mortality, myocardial infarction, or stent thrombosis after implantation of coronary drug-eluting stent, Eur. Heart J. 34 (2013) 920–931.
[18] J. Lerchner, A. Wolf, G. Wolf, I. Fernandez, Chip calorimeters for the investigation of liquid phase reactions: design rules, Thermochim. Acta 446 (2006) 168–175.
[19] R.N. Goldberg, N. Kishore, R.M. Lennen, Thermodynamic quantities for the ionization reactions of buffers, J. Phys. Chem. Ref. Data 31 (2002) 231–370.
[20] W.M. Haynes, CRC Handbook of Chemistry and Physics, 95th edition, (2015).
[21] S. Cukierman, Et tu, Grotthuss! and other unfinished stories, Biochim. Biophys. Acta 1757 (2006) 876–885.
[22] H. Buschmann, E. Schollmeyer, A test reaction from macrocyclic chemistry for calorimetric titrations, Thermochim. Acta 333 (1999) 1–5.
[23] C. Sgarlata, V. Zito, G. Arena, Conditions for calibration of an isothermal titration calorimeter using chemical reactions, Anal. Bioanal. Chem. 405 (2013) 1085–1094.
[24] T. Raj, W.H. Flygare, Diffusion studies of bovine serum albumin by quasielastic light scattering, Biochemistry 13 (1974) 3336–3340.
[25] D. Brune, S. Kim, Predicting protein diffusion coefficients, Proc. Natl. Acad. Sci. USA 90 (1993) 3835–3839.
[26] R.N. Goldberg, Y.B. Tewari, Thermodynamics of enzyme-catalyzed reactions. Part3. hydrolases, J. Phys. Chem. Ref. Data 23 (1994) 1035–1103.
[27] H.N. Fenley, P.G. Walker, Studies on alkaline phosphatase. Inhibition by phosphate derivatives and the substrate specificity, Biochem. J. 104 (1967) 1011–1018.
[28] K. Hirano, Y. Iiizumi, Y. Mori, K. Toyoshi, M. Sugiura, S. Iino, Role of alkaline phosphatase in phosphate uptake into brush border membrane vesicles from human intestinal mucosa, J. Biochem. 97 (1985) 1461–1466.